

# Effect of Oxide Additives on Phase Evolution and Tribological Behavior of Zirconia-Toughened Alumina Composite

Ashis Kumar Dey, Subrata Chatterjee, and Koushik Biswas

(Submitted December 13, 2016; in revised form July 10, 2017; published online November 10, 2017)

Four different zirconia-toughened alumina added with different pairs of oxides ( $\text{CeO}_2$ ,  $\text{TiO}_2$ ,  $\text{CuO}$ ,  $\text{ZnO}$  and  $\text{SnO}_2$ ) were prepared through the co-precipitation technique. Conventional sintering resulted in relative densities  $\geq 96\%$ . Phase analyses of these composites were performed by x-ray diffraction. Vicker's hardness and tribological behavior of all ZTA composites were studied. Microstructure analysis of polished and worn surfaces was carried out to understand and correlate the mechanical/tribological behavior with the microstructure. A different wear mechanism is observed in ZTA containing  $\text{CeO}_2$  and  $\text{TiO}_2$  which resulted in considerable improvement in tribological behavior with a minimum specific wear rate of  $9 \times 10^{-7} \text{ mm}^3/\text{Nm}$ .

**Keywords** ceramics matrix, composites, electron, microscopy, sintering, wear, x-ray

## 1. Introduction

Zirconia-toughened alumina (ZTA) ceramics have different attractive properties, including high-temperature mechanical strength, good thermal shock resistance, wear and oxidation resistance, low thermal conductivity, and corrosion resistance, which make ZTA ceramics suitable for different challenging applications like bearing components (balls, rollers and raceways), cutting tool inserts (replacing carbide and metal tools), electrosurgical insulators, valve seats, pump components, oxygen sensors, dies and biomedical applications (Ref 1, 2). It was reported in the literature (Ref 3, 4) that presence of stabilized zirconia in ZTA composite plays a significant role in the improvement in toughness by both stress-induced transformation toughening and microcrack toughening mechanism. Oxides, like  $\text{MgO}$ ,  $\text{CaO}$ ,  $\text{CeO}_2$ , and  $\text{Y}_2\text{O}_3$ , are commonly used to stabilize the tetragonal zirconia. However, with higher toughness of ZTA ceramics, it is also necessary to impart some lubricating property to the matrix for easy shear during dry sliding to make it suitable for wear resistance applications. It is also well established in the literature (Ref 5) that, for a material to be suitable for wear-resistant application in dry sliding condition, specific wear rate should be less than  $10^{-6} \text{ mm}^3/\text{Nm}$ , the coefficient of friction (COF) must be below 0.2, and the wear mechanism should be mild such that dry sliding pairs will polish each other. The wear of alumina like all other ceramic considered for wear-resistant applications may be divided into well-defined mild and severe wear zone with a narrow

transition between mild to severe (Ref 5-8). Wear properties of alumina and ceramics composite is also function of different parameters and tests condition such as: sliding distance and velocity, surface condition, contact geometry, applied load, relative humidity, surface temperature, chemical compatibility, experimental apparatus, and sample preparation technique (Ref 6). To study the wear behavior of ZTA composites in dry sliding condition different researcher used different test configuration such as: pin on disc, pin on flat, and pin on ring (Ref 5-7) using different load and sliding velocity. Different researchers also added different solid oxide lubricants in ZTA with an intention to impart a self-lubricating property to the matrix and to obtain ZTA composites with improved tribological properties without significant reduction in hardness (Ref 5, 7). Pasariu et al. (Ref 5) carried out dry sliding wear tests using commercially available alumina ball of 10 mm diameter as counter body and reported that addition of 5 wt.%  $\text{CuO}$  in alumina resulted in reduction of coefficient of friction from 0.7 to 0.4 and zirconia doped with 5 wt.%  $\text{CuO}$  resulted in reduction of coefficient of friction from 0.8 to 0.3. Kerkwijk et al. (Ref 7) studied the effects of addition (5 wt.%) of one of the soft oxides from ( $\text{ZnO}$ ,  $\text{MgO}$ ,  $\text{CuO}$ ,  $\text{B}_2\text{O}_3$ , and  $\text{MnO}_2$ ) in alumina and reported that the addition of 5 wt.%  $\text{CuO}$  to alumina matrix resulted in reduction of coefficient of friction to 0.43 with a low specific wear rate of  $10^{-7} \text{ mm}^3/\text{Nm}$  under dry sliding condition against YTZP ball as counter body. In a different study (Ref 8), authors reported that nanoscale ZTA, when dry slid against alumina ball as counter body, resulted in specific wear rate of  $10^{-9} \text{ mm}^3/\text{Nm}$ , coefficient of friction of 0.45, and the main wear mechanism was abrasion along with polishing. In view of the facts above, the present study focuses attention on the tribological behavior of ZTA added with different pair of oxides in small quantity.

## 2. Experimental

### 2.1 Materials and Synthesis

Commercially available precursor salts of the respective components, viz.,  $\text{Al}(\text{NO}_3)_3 \cdot 9\text{H}_2\text{O}$ ,  $\text{ZrO}(\text{NO}_3)_2 \cdot \text{H}_2\text{O}$ ,  $\text{Mg}(\text{NO}_3)_2 \cdot 6\text{H}_2\text{O}$ ,  $\text{Cu}(\text{NO}_3)_2 \cdot 3\text{H}_2\text{O}$ ,  $\text{Zn}(\text{NO}_3)_2 \cdot 6\text{H}_2\text{O}$ ,  $\text{TiCl}_4$ ,  $\text{Ce}(\text{NO}_3)_3 \cdot 6\text{H}_2\text{O}$ ,

Ashis kumar Dey and Subrata Chatterjee, Department of Metallurgy and Materials Engineering, Bengal Engineering and Science University, Shibpur, Howrah 711103, India; and Koushik Biswas, Department of Metallurgical and Materials Engineering, Indian Institute of Technology, Kharagpur, Kharagpur 721302, India. Contact e-mail: k\_biswas@metal.iitkgp.ernet.in.

SnCl<sub>2</sub>·2H<sub>2</sub>O, along with 30 vol.% NH<sub>4</sub>OH solution and NaOH pellets were used as starting materials. Characteristics of these chemicals are given in Table 1. The base composition of ZTA and subsequent soft-oxide-added ZTAs are synthesized from their respective salt solutions following the stoichiometry given in Table 2. The respective salts were at first dissolved in distilled water and stirred using a magnetic stirrer for 1 h. Then drop-wise NH<sub>4</sub>OH (ammoniacal) solution was added to this salt solution with continuous stirring until the pH of the solution reached to 9 and precipitation started. Precipitates were allowed to age for 48 h, and then supernatant liquid was removed by the filtration process. Precipitates were thoroughly washed with warm distilled water for complete removal of Cl<sup>-</sup> and NO<sub>3</sub><sup>-</sup> ions. AgNO<sub>3</sub> test was performed in order to ascertain complete removal of Cl<sup>-</sup> from the precipitates. Precipitates, thus obtained, were dried at 120 °C for 24 h and then calcined at 1200 °C for 1 h. Calcined powders were then ground in a crucible using mortar and pestle. Pallets ( $\phi = 8$  mm,  $h = 5$  mm) of different ZTA compositions were then prepared by compaction in a hydraulic press at a pressure of 400 MPa. The specimens were then sintered in a high-temperature PID-controlled resistance-heated furnace at 1600 °C for 2 h. Flow diagram of the synthesis process for different types of ZTA powders is shown in Fig. 1.

## 2.2 Characterization of Ceramics

Green density ( $\rho_G$ ) of different specimen was calculated by dividing mass of each pallet by its volume, and volume of each pallet was determined from its dimension. Theoretical density ( $\rho_{Th}$ ) of the different composite system was calculated considering the different phases formed after sintering as identified by XRD analysis. Sinter density ( $\rho_s$ ) and relative density ( $\rho_{rel}$ ) of the specimen were measured using the equations described elsewhere (Ref 9). Densification parameter ( $D$ ) for each specimen was measured using Eq 1.

$$D = \frac{\rho_s - \rho_G}{\rho_{Th} - \rho_G} \quad (\text{Eq 1})$$

Sintered specimens of different ZTA composites were initially coarse-polished using SiC abrasive grit paper (grade 600,800,1000,1200,1600) and then finally diamond-polished up to 1- $\mu$ m surface finish. Vickers indentation hardness was measured for different composite system applying a load of 10 kgf keeping a holding time 20 s. For each specimen, 12 readings for hardness data were taken. X-ray diffraction (XRD) was performed in Philips x-ray diffractometer (PW 1840, Holland) using filtered Cu K $\alpha$  radiation ( $\lambda = 0.15406$  nm) for powders obtained after calcinations and sintered specimens of different composition. Qualitative phase analysis was carried out with the help of X-Pert High score Plus<sup>TM</sup> software, which

uses the ICDD database for crystallographic information. Microstructures of polished sintered surfaces (1- $\mu$ m surface finish) were studied by scanning electron microscopy (Zeiss supra 40 attached with oxford energy-dispersive x-ray micro-analysis). To avoid charging effect under SEM, specimens were sputtered with gold.

## 2.3 Tribology

Tribological behavior of the sintered and polished specimens (surface finish of 1  $\mu$ m) was studied using multi-tribometer (Phoenix, UK). Pin-shaped ( $\phi = 6$  mm) specimen was used against alumina disk as counter body during the wear test. Wear depths and coefficient of frictions were measured at a velocity of 0.275 m/s with a load of 30 N for a maximum sliding distance of 2.5 km. Specific wear rates of different ZTA composites were measured using the equation given below.

$$K_w = \frac{V_w}{F \cdot S} \left( \frac{\text{mm}^3}{\text{Nm}} \right) \quad (\text{Eq 2})$$

where  $K_w$  is the specific wear rate,  $V_w$  is the wear volume,  $F$  is the applied force (N), and  $S$  is the sliding distance (m). Mass loss was calculated by measuring the mass of the specimen, before and after the wear test. Wear volume ( $V_w$ ) was calculated from the mass loss data. Cumulative wear depth of the specimens and their coefficient of frictions were obtained directly from the machine interfaced with computer aided data recorder.

## 3. Results and Discussion

### 3.1 Phase Analysis of Calcined Powder (Precipitated)

XRD analyses of calcined powders are shown in Fig. 2(a) and (b). The matrix phase Al<sub>2</sub>O<sub>3</sub> is present as metastable  $\theta$ -phase (monoclinic) (ICDD 00-023-1009) in composite systems C1 and C4 and as stable  $\alpha$ -phase (ICDD 00-043-1484) in composite systems C6 and C9. The absence of strong  $\alpha$ -alumina is obvious from Fig. 2(a). It also reveals the presence secondary phase ZrO<sub>2</sub> in both tetragonal (t-ZrO<sub>2</sub>, ICDD 01-079-1764) and monoclinic (m-ZrO<sub>2</sub>, ICDD 01-078-0047) form in all composite systems. XRD results also confirm the presence of cubic MgO and spinel MgAl<sub>2</sub>O<sub>4</sub> (ICDD 00-001-1157) in composite systems C1, C6, and C9. However, MgO could not be detected in the composite system C4 as it is possibly consumed during formation of MgAl<sub>2</sub>O<sub>4</sub> spinel. It is noteworthy that both CeO<sub>2</sub> (ICDD 01-075-0076) and SnO<sub>2</sub> (ICDD 01-077-0452) were present in this system C4, whereas, in system C9, CuO and ZnO were not detected and all the

**Table 1** Characteristics of starting chemicals

Chemical name	Chemical formulae	Molecular weight, gm/mol	Purity	Source
Aluminum nitrate nonahydrate	Al(NO <sub>3</sub> ) <sub>3</sub> ·9H <sub>2</sub> O	375.13	≥ 95%	E. Merck, India
Magnesium nitrate hexahydrate Purified	Mg(NO <sub>3</sub> ) <sub>2</sub> ·6H <sub>2</sub> O	256.41	≥ 99%	
Copper (II) nitrate trihydrate	Cu(NO <sub>3</sub> ) <sub>2</sub> ·3H <sub>2</sub> O	241.60	≥ 99%	Loba Chemie, India
Zinc nitrate hexahydrate	Zn(NO <sub>3</sub> ) <sub>2</sub> ·6H <sub>2</sub> O	297.47	≥ 99.5%	
Zirconyl nitrate	ZrO(NO <sub>3</sub> ) <sub>2</sub> ·H <sub>2</sub> O	249.24	Practical grade	
Titanium tetrachloride	TiCl <sub>4</sub>	189.71	≥ 99.5%	
Cerous nitrate	Ce(NO <sub>3</sub> ) <sub>3</sub> ·6H <sub>2</sub> O	434.23	≥ 99.9%	
Stannous chloride	SnCl <sub>2</sub> ·2H <sub>2</sub> O	225.63	97%	

**Table 2** Specification of starting powders

Powder denomination	Additive oxides, wt. %	Al <sub>2</sub> O <sub>3</sub> , wt. %	ZrO <sub>2</sub> , wt. %	MgO, wt. %
C1	...	77.60	19.40	3
C4	CeO <sub>2</sub> -4, SnO <sub>2</sub> -4	71.4	17.85	2.75
C6	CeO <sub>2</sub> -4, TiO <sub>2</sub> -4			
C9	CuO-4, ZnO-4			

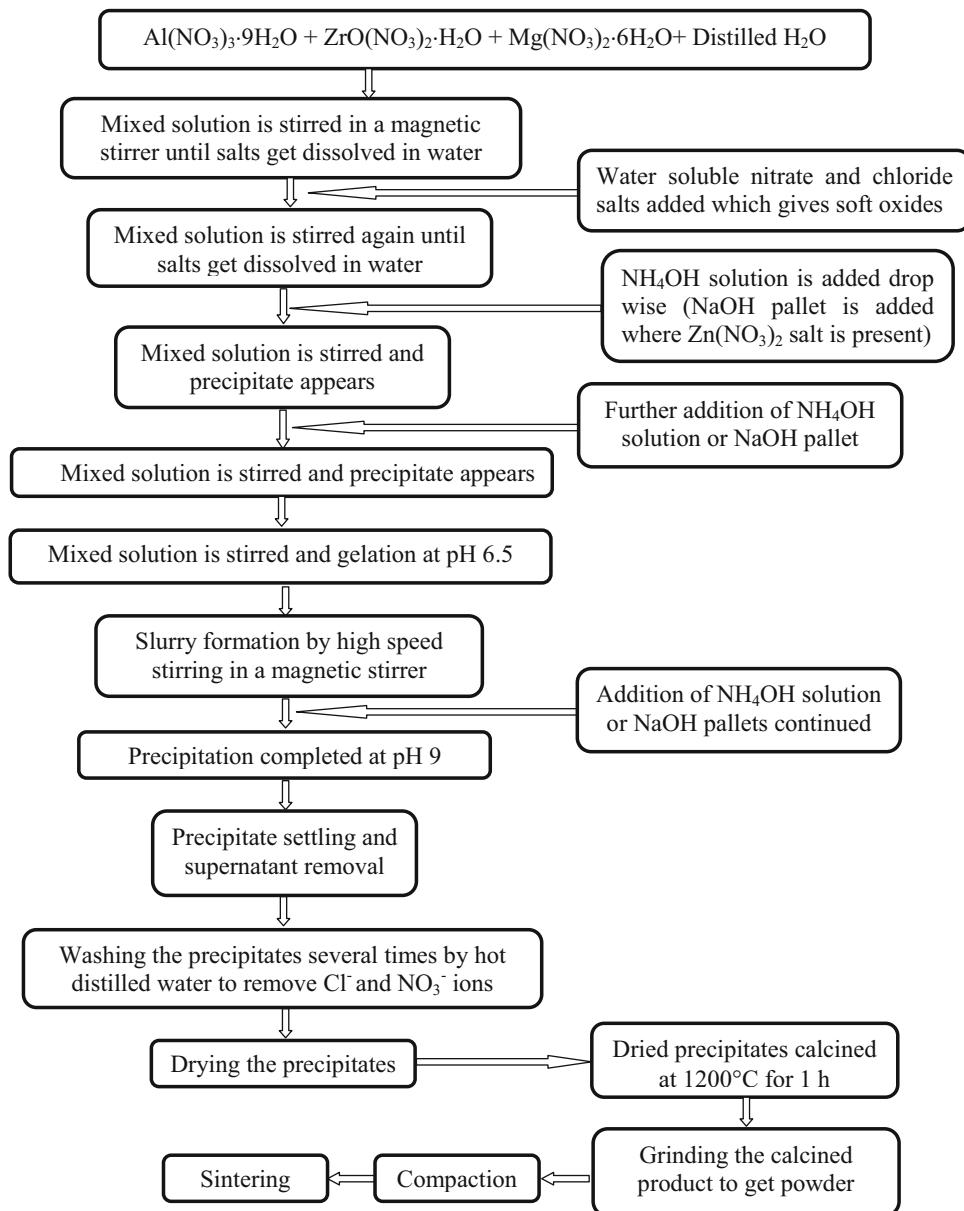


**Fig. 1** Flowchart for preparation ZTA nano-composites with and without additive oxides

major peaks belongs to CuAl<sub>2</sub>O<sub>4</sub> (ICDD 01-078-1605) and ZnAl<sub>2</sub>O<sub>4</sub> (ICDD 01-073-1961) as shown in Fig. 2(b). Like C4, presence of additive oxides CeO<sub>2</sub> and TiO<sub>2</sub> (ICDD 00-034-0180) were also detected in C6 system. Since solubility of either CeO<sub>2</sub> or TiO<sub>2</sub> in Al<sub>2</sub>O<sub>3</sub> at around 1200 °C is very low (Ref 10-12), these additives are present unreacted in the matrix.

In contrast, CuO and ZnO additives in system C9 readily form CuAl<sub>2</sub>O<sub>4</sub> and ZnAl<sub>2</sub>O<sub>4</sub> spinel phases at moderate temperatures (around 900-1000 °C) following the reactions, respectively (Ref 13):



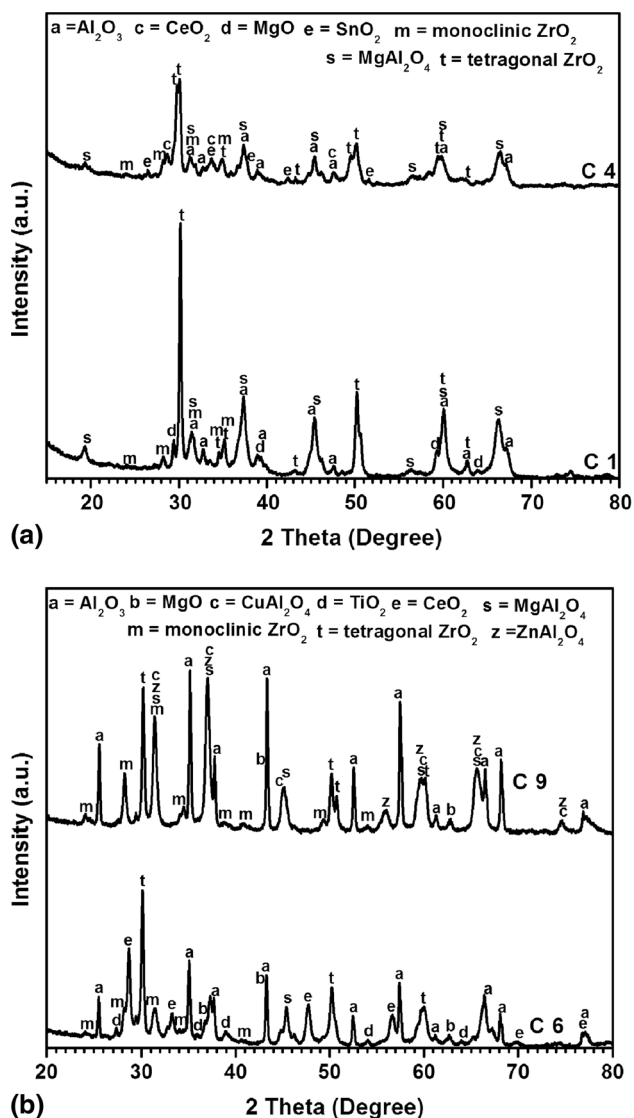
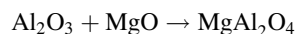


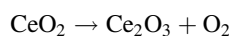
Fig. 2 X-ray diffraction patterns of calcined powder for composite systems. (a) C1 and C6, (b) C4 and C9

### 3.2 Sintering, Densification, Microstructure, and Phase Evolution

The composite systems were sintered at 1600°C for 2 h, and all of them were having density > 95% of the theoretical one. The sintered density of the different composite systems is reported in Table 3. Maximum relative density of 98.5% was obtained for the composite system C6, and minimum of 95.5% was measured for the system C9. Lower density in system C9 is primarily attributed to the volatilization of CuO and ZnO at 1600 °C. However, volatilization loss of SnO<sub>2</sub> in system C4 is limited as decomposition is somewhat suppressed by the presence of MgO due to possible spinel formation (Ref 14). XRD result, however, lacks the evidence of Mg<sub>2</sub>SnO<sub>4</sub> (or might be below the level of detection) in this system. XRD for all the sintered composite system, as shown in Fig. 3(a) and (b), confirms the presence of a minor phase MgAl<sub>2</sub>O<sub>4</sub> (a reaction product between MgO and Al<sub>2</sub>O<sub>3</sub>) in all composite system except C6. Formation of MgAl<sub>2</sub>O<sub>4</sub> for all composite system can be explained from the equation given below at high sintering temperature of 1600 °C.

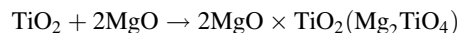
Standard Gibbs free energy of spinel MgAl<sub>2</sub>O<sub>4</sub> formation for solid-state reaction is given by Ref 15 ( $\Delta G = -35600 - 2.09T$  J/mol) and at 1600 °C,  $\Delta G = -39514.57$  J/mol < 0 which fulfill the thermodynamic requirement of formation of MgAl<sub>2</sub>O<sub>4</sub>. It was also reported that MgO in alumina matrix acted as a strong grain growth inhibitor and promoted the sintering of Al<sub>2</sub>O<sub>3</sub> (Ref 16). Presence of MgAl<sub>2</sub>O<sub>4</sub> also contributed to the suppression of grain growth by acting as a pinning agent (Ref 17). It also accelerates sintering kinetics by creating anionic vacancies (aliovalent substitution) which help diffusion and thus achieve faster densification. Unstable  $\theta$ -Al<sub>2</sub>O<sub>3</sub> (monoclinic), present in calcined powders (in C1 and C4 systems), gets converted to stable  $\alpha$ -Al<sub>2</sub>O<sub>3</sub> after sintering at higher temperatures. For sintered specimen of composite system C6 and C9, matrix phase is observed to be also stable  $\alpha$ -Al<sub>2</sub>O<sub>3</sub>. It was also observed that zirconia is present in only monoclinic form in all the composite system.

XRD analysis of system C4 (Fig. 3b) reveals the presence of minor phases like MgAl<sub>2</sub>O<sub>4</sub> and CeAl<sub>11</sub>O<sub>18</sub> (ICDD 00-048-0055). Literature shows that formation of CeAl<sub>11</sub>O<sub>18</sub> occurs following reaction between Al<sub>2</sub>O<sub>3</sub> and CeO<sub>2</sub> in the temperature range of 1200-1400 °C (Ref 10, 11). Initially, CeO<sub>2</sub> is reduced to Ce<sub>2</sub>O<sub>3</sub> and then further reacted with alumina to form CeAl<sub>11</sub>O<sub>18</sub> following these reactions:



It was also reported in literature (Ref 10) that alumina added with yttria-stabilized zirconia (YSZ) composites containing 3-5 wt.% ceria sintered at 1400 °C resulted in a composite with 99% relative density along with the formation of elongated grains of CeAl<sub>11</sub>O<sub>18</sub> within alumina matrix. In another study (Ref 11), it was also reported that ZTA-MgO composite when added with 1 wt.% CeO<sub>2</sub> resulted in maximum density and an increase in CeO<sub>2</sub> content (5 wt.%) resulted in reduction of density due to the formation of elongated grains of CeAl<sub>11</sub>O<sub>18</sub>.

XRD analysis for the composite system C6, as shown in Fig. 3(a), confirms the formation of different minor phases, viz., CeAl<sub>11</sub>O<sub>18</sub> and cubic Mg<sub>2</sub>TiO<sub>4</sub> (ICDD 00-003-0858) along with  $\alpha$ -Al<sub>2</sub>O<sub>3</sub> as matrix and m-ZrO<sub>2</sub> as secondary phase. MgO-TiO<sub>2</sub> phase diagram (Ref 18) reveals that temperature in excess of 1500°C favors the formation of cubic Mg<sub>2</sub>TiO<sub>4</sub> following the reaction:



It was also reported (Ref 19) that above 1300°C, excess TiO<sub>2</sub> beyond its solid solubility limit (~0.3 wt.%) in MgO reacted with MgO to form inter- and intragranular Mg<sub>2</sub>TiO<sub>4</sub> phase. Decomposition of this high-temperature phase during cooling at lower temperature was also reported according to the following reaction.



However, without any doping agent, this high-temperature phase can also be retained at room temperature even after slow cooling (Ref 20) and present observation is also similar to the result reported earlier. Previous study (Ref 12) have reported that TiO<sub>2</sub> in Al<sub>2</sub>O<sub>3</sub> above 1200°C do form a metastable Al<sub>2</sub>TiO<sub>5</sub> stoichiometric compound, however, during



**Table 3 Sintered and relative density of different ZTA composite systems**

Composite system	Theoretical density, g/cm <sup>3</sup>	Green density, g/cm <sup>3</sup>	Sintered density, g/cm <sup>3</sup>	% relative density	Densification parameter ( <i>D</i> )
C1	4.16	2.10	4.06	97.6	0.95
C4	4.24	2.20	4.19	97.4	0.97
C6	4.16	2.21	4.10	98.5	0.97
C9	4.23	2.39	4.04	95.5	0.90

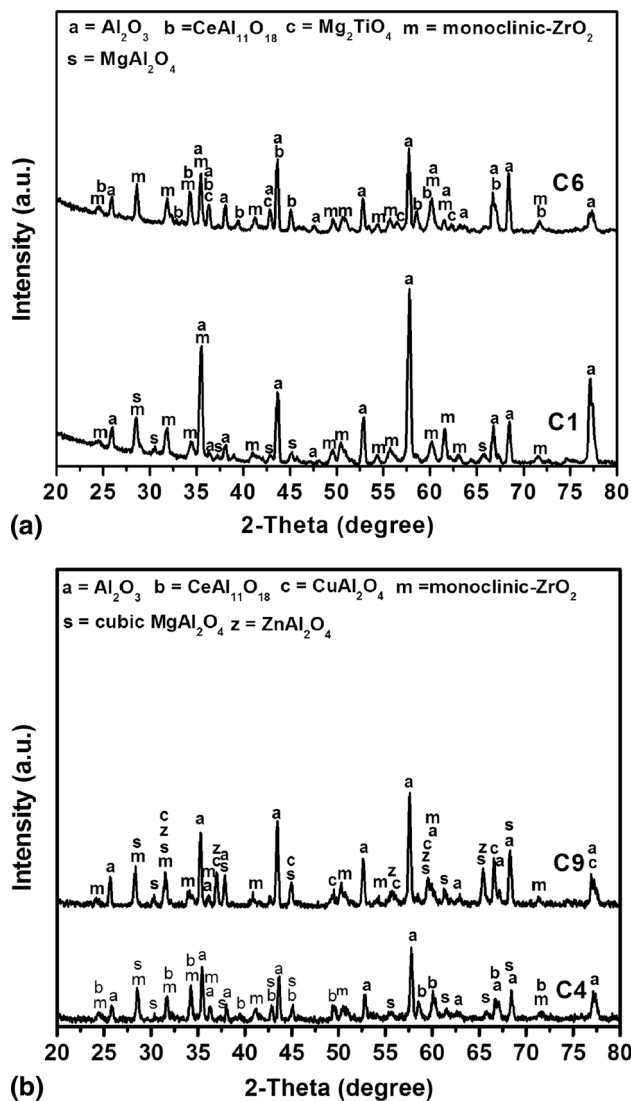
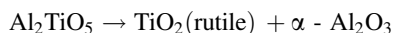


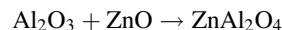
**Fig. 3** X-ray diffraction patterns of sintered composite systems. (a) C1 and C6, (b) C4 and C9

cooling from the sintering temperature, it decomposes back to TiO<sub>2</sub> in Al<sub>2</sub>O<sub>3</sub> as per the eutectoid reaction:



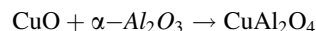
In the composite system C9, presence of the two volatile oxides (ZnO and CuO) (having high vapor pressure) may have resulted in less dense sintered body in comparison with other composite systems. However report (Ref 14) suggests that decomposition of SnO<sub>2</sub> is somewhat suppressed by the presence of MgO due to possible spinel. XRD analysis

(Fig. 3b) of this composite system confirms the formation of different minor phases, viz., MgAl<sub>2</sub>O<sub>4</sub>, ZnAl<sub>2</sub>O<sub>4</sub> (ICDD 00-001-1146) and CuAl<sub>2</sub>O<sub>4</sub> (ICDD 00-001-1153) along with matrix ( $\alpha$ -Al<sub>2</sub>O<sub>3</sub>) and secondary phase (m-ZrO<sub>2</sub>). Formation of Zn spinel occurs following the equation:



Gibbs free energy change for the reaction given by Jacob et al. (Ref 21) as  $\Delta G^0 = -45.0081 + 0.0066T$  (in kJ/mol) indicates the favorable condition for formation of ZnAl<sub>2</sub>O<sub>4</sub> from room temperature to 1600 °C.

Formation of CuAl<sub>2</sub>O<sub>4</sub> takes place according to the following reaction:



Gibbs free energy change for the reaction is given by Jacob et al. (Ref 22) as  $\Delta G = 4403 - 4.97T$  (in cal/mol), and they predicted the possible formation of stable CuAl<sub>2</sub>O<sub>4</sub> above 612 °C. Recently, published literature (Ref 23) reported that CuO react with  $\alpha$ -Al<sub>2</sub>O<sub>3</sub> to form CuAl<sub>2</sub>O<sub>4</sub> above 1000 °C. Another study (Ref 24) reports that CuAl<sub>2</sub>O<sub>4</sub> undergoes decomposition within 1000-1400 °C according to following reaction.



It was also reported in literature (Ref 25) that excess  $\alpha$ -Al<sub>2</sub>O<sub>3</sub> within matrix suppresses the decomposition of CuAl<sub>2</sub>O<sub>4</sub> and increases the thermal stability of the spinel phase.

SEM micrograph of the sintered and polished composite specimen C1 shown in Fig. 4(a) reveals the formation of nearly dense composite where dark phases are alumina-rich and bright phases are zirconia-rich ones. SEM images of C4, as shown in Fig. 4(b), reveals that zirconia phases (white grains) are well dispersed within the  $\alpha$ -Al<sub>2</sub>O<sub>3</sub> matrix along with the presence of elongated grains of CeAl<sub>11</sub>O<sub>18</sub>. EDS analysis of the respective phase also confirms the formation of CeAl<sub>11</sub>O<sub>18</sub>. Figure 4(c) represents the SEM structure of C6 composite showing a dense microstructure with well-dispersed bright secondary ZrO<sub>2</sub> phase within dark alumina matrix phase. The matrix grains were rather large compared to other systems owing to the fact that the addition of TiO<sub>2</sub> promotes grain growth of Al<sub>2</sub>O<sub>3</sub> (Ref 12). All TiO<sub>2</sub> reacted with MgO to form Mg<sub>2</sub>TiO<sub>4</sub>, and as a result, there was no evidence of formation of MgAl<sub>2</sub>O<sub>4</sub> in C6 which also contributed to grain coarsening effect. SEM micrograph of C9 (shown in Fig. 4d) shows the presence of well-dispersed zirconia grains within alumina matrix along with the presence of different spinels (ZnAl<sub>2</sub>O<sub>4</sub> and CuAl<sub>2</sub>O<sub>4</sub>) formed. Results of EDS analysis also gives the evidence of formation of spinels. The matrix grain size in this system is found to very fine as ZnAl<sub>2</sub>O<sub>4</sub> spinel dopant acted as a grain growth inhibitor in the alumina system (Ref 14).

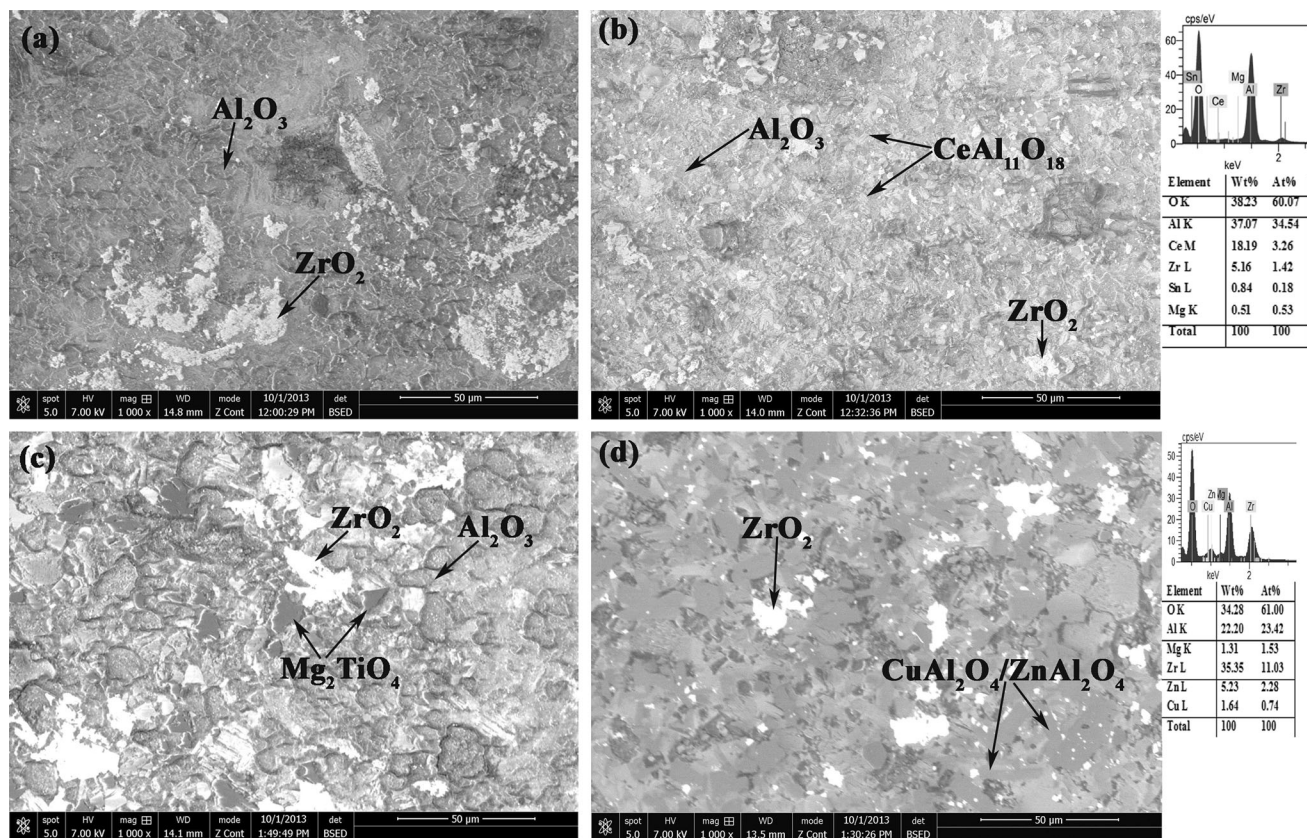


**Fig. 4** SEM micrograph of polished surface of composite system. (a) C1, (b) C4, (c) C6, and (d) C9

### 3.3 Hardness of the Composite Systems

Vickers hardness values for different ZTA composite systems are given in Table 4. As expected, maximum hardness of  $16.78 \pm 2.98$  GPa was obtained for composite system C1 (without any soft additive oxides). Volume fractions of different phases formed in sintered specimen of ZTA composite C1 are  $\alpha$ -Al<sub>2</sub>O<sub>3</sub>  $\approx$  74%, ZrO<sub>2</sub>  $\approx$  13.8%, and MgAl<sub>2</sub>O<sub>4</sub>  $\approx$  12.2%. It was reported (Ref 1) that the addition of relatively softer phase zirconia to a harder matrix phase alumina resulted in lowering of the hardness of the composites. Literature (Ref 26) reports that Vickers' hardness values for MgAl<sub>2</sub>O<sub>4</sub> are in the range of 14-17 GPa. Vickers' hardness value for  $\alpha$ -Al<sub>2</sub>O<sub>3</sub> and monoclinic ZrO<sub>2</sub> phases are 20 and 12 GPa, respectively. Composite system C6 (contains CeO<sub>2</sub> and TiO<sub>2</sub> as additives) exhibited Vickers hardness value of  $14.46 \pm 1.83$  GPa. Volume fraction of different phases formed after sintering are  $\alpha$ -Al<sub>2</sub>O<sub>3</sub>  $\approx$  62%, monoclinic ZrO<sub>2</sub>  $\approx$  13%, Mg<sub>2</sub>TiO<sub>4</sub>  $\approx$  6.5%, CeAl<sub>11</sub>O<sub>18</sub>  $\approx$  17.5%, and unreacted TiO<sub>2</sub>  $\approx$  1%. Reduction in hardness value of composite system C6 in comparison with C1 (base composition) may be due to reduction in the volume fraction of the  $\alpha$ -Al<sub>2</sub>O<sub>3</sub> content in C6. Formation of different other phases viz., Mg<sub>2</sub>TiO<sub>4</sub> (hardness value  $\approx$  10 GPa) and CeAl<sub>11</sub>O<sub>18</sub> (hardness value greater than zirconia but lower than alumina) also gives clear indication of the lower hardness value. Addition of CeO<sub>2</sub> and SnO<sub>2</sub> as additive oxides for the composite system C4 resulted in Vickers hardness value of  $14.15 \pm 2.03$  GPa. Different secondary phases formed in C4 were MgAl<sub>2</sub>O<sub>4</sub> and CeAl<sub>11</sub>O<sub>18</sub>. Volume fraction of different phases formed after sintering are  $\alpha$ -Al<sub>2</sub>O<sub>3</sub>  $\approx$  56.72%, monoclinic ZrO<sub>2</sub>  $\approx$  13.26%, MgAl<sub>2</sub>O<sub>4</sub>  $\approx$  9.78% and CeAl<sub>11</sub>O<sub>18</sub>

17.76% and unreacted SnO<sub>2</sub>  $\approx$  2.48%. Further reduction in the volume fraction of alumina and consequent increase in the volume fraction of the comparative softer phases might have resulted in obtaining reduced hardness value for the composite system C4. Similar observations (Ref 11, 27) were also reported for ceria-added alumina composite in different study. Rejab et al. (Ref 11) reported that addition of 7 wt.% ceria in ZTA with composition (80 wt.% Al<sub>2</sub>O<sub>3</sub> + 20 wt.% YSZ) added with 0.7 wt.% MgO resulted in the reduction of hardness from 14.99 to 14.15 GPa due to the formation of secondary phase CeAl<sub>11</sub>O<sub>18</sub>. Another study carried out by Magalaraja et al. (Ref 27) reported that the addition of 5 vol.% ceria in ZTA (Al<sub>2</sub>O<sub>3</sub>-10 vol.% 3YTZP) resulted in the reduction of hardness from 14.51 to 12.62 GPa. Compared to rest of composite systems, considerable reduction in hardness ( $\approx 13.10 \pm 2.25$  GPa) was measured for the composite system C9. The major factor causing such drop is the lower sintered density (about 95% rel. density). Apart from that, different spinel phases (CuAl<sub>2</sub>O<sub>4</sub> and ZnAl<sub>2</sub>O<sub>4</sub>) formed in this composite system also attributes to low hardness. Literature (Ref 28) shows that polycrystalline ZnAl<sub>2</sub>O<sub>4</sub> has lower hardness of 10.5 GPa. Hardness value of CuAl<sub>2</sub>O<sub>4</sub> is similar to that of ZnAl<sub>2</sub>O<sub>4</sub>. Volume fractions of different phases formed after sintering, as evident from XRD results, are  $\alpha$ -Al<sub>2</sub>O<sub>3</sub>  $\approx$  59%, monoclinic ZrO<sub>2</sub>  $\approx$  13.05%, MgAl<sub>2</sub>O<sub>4</sub>  $\approx$  11.43%, CuAl<sub>2</sub>O<sub>4</sub> 8.18%, and ZnAl<sub>2</sub>O<sub>4</sub>  $\approx$  8.34%. Thus, major harder matrix phase alumina, when reacted with different other oxides (MgO, CuO and ZnO), forms different spinel phases which are comparatively softer than alumina and consequently resulted in low hardness value of the composite system C9.



**Table 4** Vickers hardness number for different composite systems

Composite system	C1	C4	C6	C9
Vickers' Hardness number, GPa	16.78 ± 2.98	14.15 ± 2.03	14.46 ± 1.83	13.10 ± 2.25

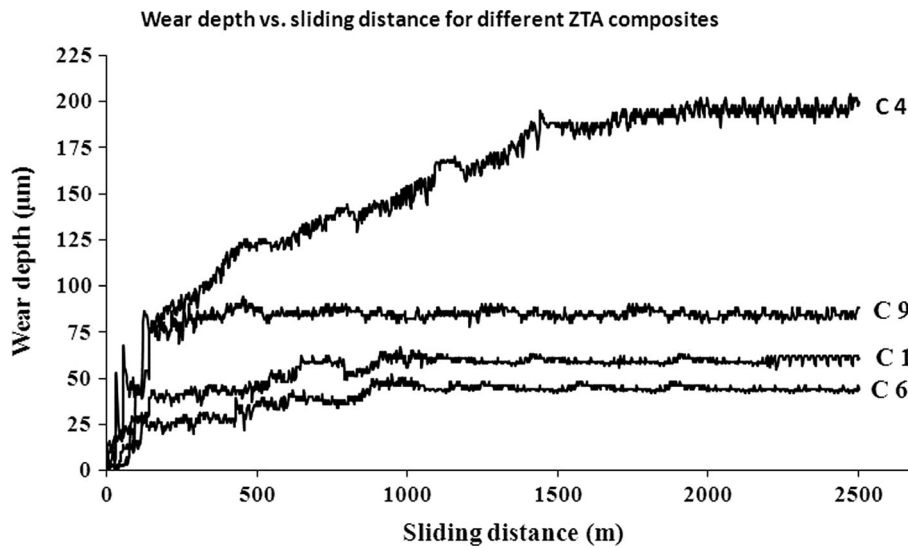


**Fig. 5** Cumulative wear depth vs. sliding distance for different ZTA composites

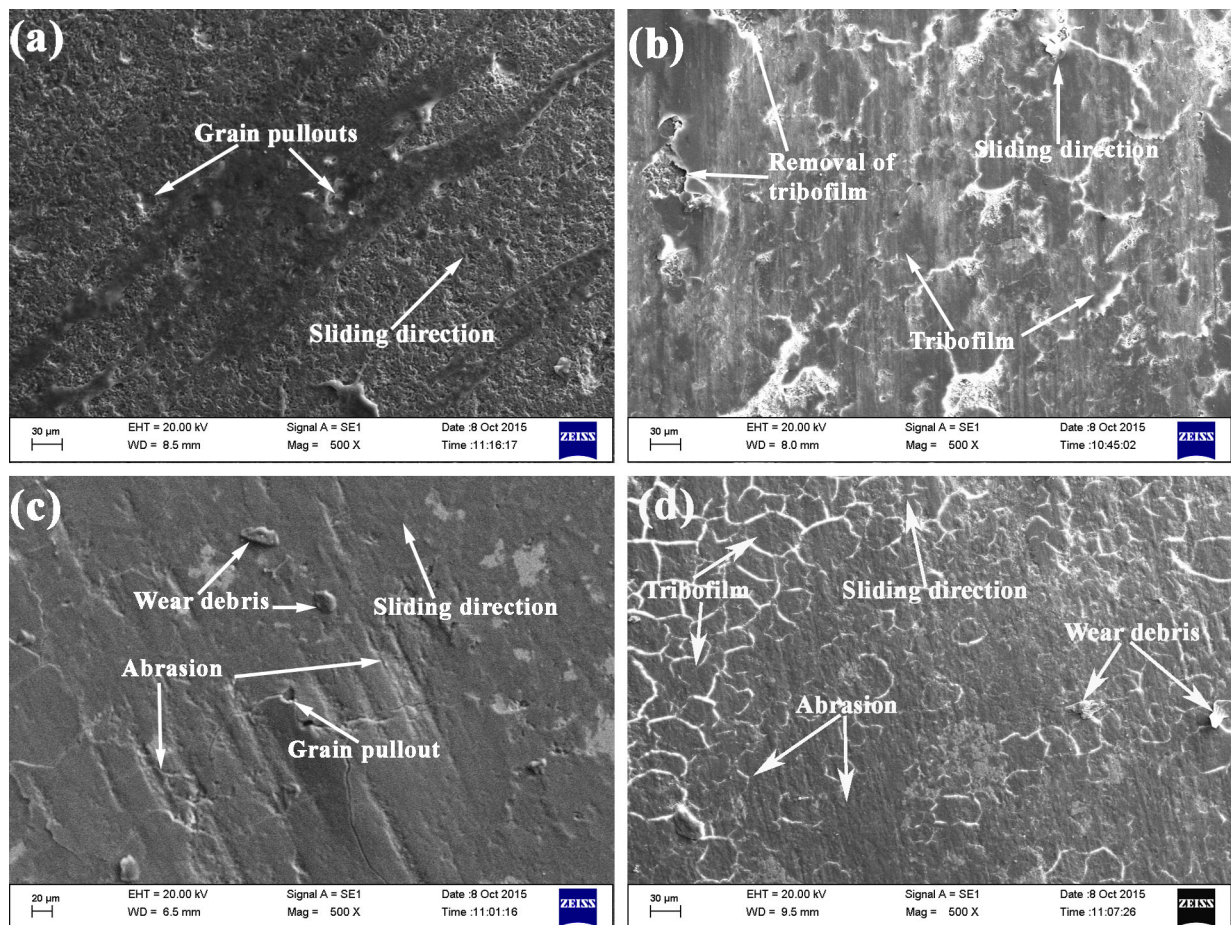


**Fig. 6** SEM micrograph of the worn surface of the composite system (a) C1, (b) C4, (c) C6, and (d) C9

### 3.4 Tribological Behavior

Severity of the dry sliding wear behavior of alumina composites against alumina as counter body primarily depends on applied load, sliding velocity, contact geometry of the sliding pairs, and test configuration. An organized dry sliding wear test for alumina composite against alumina cylindrical pin with a hemispherical tip of radius 2.75 mm was carried out to determine the critical condition for wear transition from mild wear to severe wear and reported to observe clear transition from mild to severe wear at normal load of 30 N and sliding speed of 0.37 m/s (Ref 29). Present study was carried out with a normal load of 30 N and sliding speed of 0.275 m/s which may be considered as a mild wear region based on the result of the previous study (Ref 29). Cumulative wear depths recorded for different ZTA composite systems are shown in Fig. 5. Maximum wear depth of 202  $\mu\text{m}$  for ZTA composite system C4 (contains  $\text{CeO}_2$  and  $\text{SnO}_2$  as additives) and the minimum wear depth of 44  $\mu\text{m}$  for ZTA composite system C6 (contains  $\text{CeO}_2$  and  $\text{TiO}_2$  as additives) were recorded, whereas ZTA composite system C1 (without additives) resulted in wear depth of 60  $\mu\text{m}$ . ZTA composite system C9 (contains  $\text{ZnO}$  and  $\text{CuO}$  as additives) exhibited a wear depth of 88  $\mu\text{m}$ . Specific wear rate for different composite systems are given in Table 2. Maximum specific wear rate was recorded for the composite system C4, and minimum specific wear rate was obtained for the composite system C6.

Steady-state condition was achieved after a dry sliding distance of 1 km for the ZTA composite systems C1 and C6. Composite system C9 quickly attained a steady-state condition after sliding a very short distance of 200 m, but for composite system C4, steady-state condition was observed after a distance of 1.75 km.

Wear depth of 60  $\mu\text{m}$  and the specific wear rate of  $1.5 \times 10^{-6} \text{ mm}^3/\text{Nm}$  were obtained for the composite system C1 after dry sliding the specimen for a distance of 2.5 km.

Removal of wear debris from the alumina disc during dry sliding wear test was not observed for any of the specimen. SEM micrograph of the worn surface of the composite system C1 (without additive oxides; Fig. 6a) reveals that mild abrasion along with grain pullouts is the main wear mechanism.

Addition of  $\text{CeO}_2$  and  $\text{SnO}_2$  as additive oxides in composite system C4 did not result in any significant improvement in its tribological properties and a very high specific wear rate of  $3 \times 10^{-5} \text{ mm}^3/\text{Nm}$  (five times higher in comparison with that of the base composition) was recorded. SEM micrograph of the worn surface, as shown in Fig. 6(b), shows the formation of thin layers, which is known as tribofilm, consisting of fine grain size particles (wear debris). Wear debris are formed due to continuous removal of small particle from the specimen under test. Small particles clustered together and formed large lumped with porosity and cracks. Debris gets compacted on the wear surface and also fills the voids and grooves created during dry sliding. Wear surface also reveals the presence of extensive microcracks on the tribofilm. There was also indication of removal of the tribofilm from the wear surface and resulted in exposure of new rough surface. Complete removal of cracked tribofilm resulted in high wear rate of the composite system.

Addition of  $\text{CeO}_2\text{-TiO}_2$  as additive oxides in the composite system C6 resulted in the considerable improvement in tribological properties of the composite system. Minimum specific wear rate of  $9 \times 10^{-7} \text{ mm}^3/\text{Nm}$  was recorded for the composite system. SEM micrograph, as shown in Fig. 6(c), for the worn surface of the composite system C6 reveals that plastic deformation occurred along with mild abrasion and occasional grain pullouts. Conventionally, in alumina ceramics, grain coarsening has been found to improve the crack growth resistance characteristics. Although larger grain size reported to degrade the wear behavior, but change in major wear mechanism for C6 composite system may attributed high wear resistance compared to the other systems. Addition of comparatively soft oxides  $\text{CuO}$  and  $\text{ZnO}$  as additive oxides in

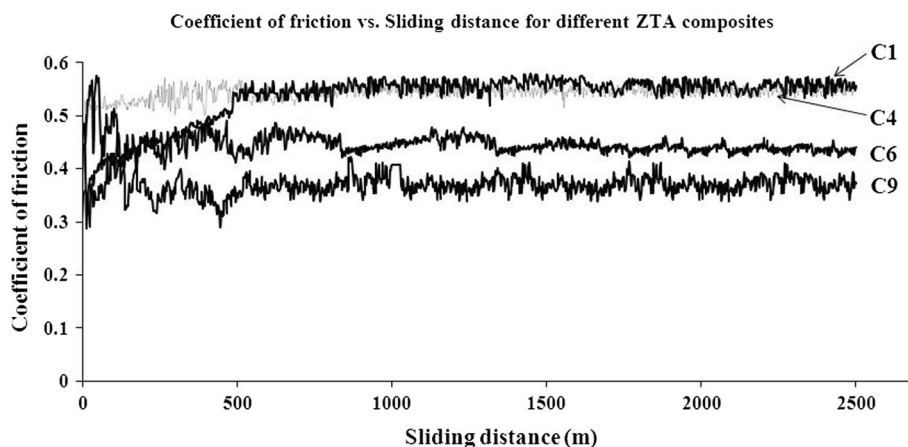


Fig. 7 Coefficient of friction (C.O.F) for different ZTA composite systems

Table 5 Specific wear rates and coefficient of friction for different composites

Composite system	C1	C4	C6	C9
Specific wear rate, $\text{mm}^3/\text{Nm}$	$1.5 \times 10^{-6}$	$3 \times 10^{-5}$	$9 \times 10^{-7}$	$2.9 \times 10^{-6}$
Coefficient of friction	0.54-0.57	0.53-0.57	0.44-0.47	0.35-0.38



composite system C9 resulted in specific wear rate of almost twice that of the base composition C1. SEM micrograph of the worn specimen in Fig. 6(d) reveals the formation of tribofilm on the worn surface due to the compaction of wear debris on the worn surface. Comparatively stable tribofilm formed on the worn surface due to the presence of different softer phases like  $ZnAl_2O_4$  and  $CuAl_2O_4$  resulted in low specific wear rate of C9 in comparison with C4. Mild abrasion along with occasional grain pullouts of different phases is the main wear mechanism.

### 3.5 Coefficient of Friction

The variation in coefficient of friction for different composite system is shown in Fig. 7. Maximum C.O.F. of 0.54-0.57 was observed for C1 (without additive). Minimum C.O.F. (0.35-0.38) was observed for composite system C9 (contains relatively softer CuO and ZnO as additives). Addition of  $CeO_2$  and  $SnO_2$  as additives in ZTA composite C4 did not result in any significant reduction in C.O.F. Though there was formation of tribofilm on the wear surface but quick removal of that due to absence of any comparatively softer phases resulted in exposure of new rough surface and as a result of which higher C.O.F. was obtained. For composite system, C6 added with  $CeO_2$ - $TiO_2$  as additives resulted in C.O.F. in the range of 0.44-0.47. Formation of relatively softer  $Mg_2TiO_4$  (6.5 vol.%) in C6 probably contributed in the slight reduction of C.O.F. Presence of comparatively softer phases viz.,  $CuAl_2O_4$  and  $ZnAl_2O_4$  (with total large volume fraction  $\approx 17$ ) in composite system C9 contributed to the formation of relatively stable tribofilm (in comparison with C4) and resulted in lower C.O.F. (Table 5).

## 4. Conclusions

Base composition of ZTA designated as C1 exhibited high C.O.F. in the range of 0.54-0.57 along with specific wear rate of  $1.5 \times 10^{-6} \text{ mm}^3/\text{Nm}$ . Main wear mechanism was observed for C1 as abrasion with occasional grain pullouts. Addition of  $CeO_2$  and  $SnO_2$  in the composite system C4 did not contribute in any improvement in the tribological properties. Composite system C9 added with 4 wt.% each of CuO and ZnO as additives resulted in significant reduction of C.O.F. in the range of 0.35-0.38 but with high specific wear rate of  $2.9 \times 10^{-6} \text{ mm}^3/\text{Nm}$ . Formation comparatively large volume fraction ( $\approx 17\%$ ) of softer phases like  $CuAl_2O_4$  and  $ZnAl_2O_4$  in C9 contributed significantly for low C.O.F. For both C4 and C9, there was formation of tribofilm on the wear surface due to compaction of wear debris on the wear surface but tribofilm film formed on wear surface of C9 is relatively stable than in C4. ZTA composite system C6 added with 4 wt.% each of  $TiO_2$  and  $CeO_2$  as additive oxides resulted in obtaining high dense (98.5% rel. density) sintered body and slightly reduced C.O.F. in the range of 0.44-0.48 with lowest specific wear rate of  $9 \times 10^{-7} \text{ mm}^3/\text{Nm}$ . Mild abrasion along with occasional grain pullouts and plastic deformation was the main wear mechanism under dry sliding condition against alumina as counter body. Based on the above findings it may be concluded that ZTA composite added with small amount of  $CeO_2$  and  $TiO_2$  (4 wt.% each) may be suitable material for wear resistance applications.

## References

1. D. Sarker, S. Adak, and N.K. Mitra, Preparation and Characterization of  $Al_2O_3$ - $ZrO_2$  Nanocomposites, Part I: Powder Synthesis and Transformation Behaviour During Fracture, *Compos. A Appl. Sci.*, 2007, **38**, p 124–131
2. J.F. Bartolome, A.H. De Aza, A. Martin, Y. Pastor, J. Llorea, R. Torrecillas, and G. Bruno, Alumina/Zirconia Micro/Nanocomposites: A New Material for Biomedical Applications with Superior Sliding Wear Resistance, *J. Am. Ceram. Soc.*, 2007, **90**, p 3177–3184
3. D. Sarker, S. Adak, M.C. Chu, S.J. Cho, and N.K. Mitra, Influence of  $ZrO_2$  on the Thermo-mechanical Response of Nano-ZTA, *Ceram. Int.*, 2007, **33**, p 255–261
4. A. Mohd Ali, A.Z.A. Azhar, N.S. Abdullah, M.M. Ratnam, and Z.A. Ahmad, Tetragonal and Monoclinic Phase Transformation of ZTA-MgO Ceramic Cutting Tool by Machining Process, in *Materials Science Forum*, Z.A. Ahmad, M.Y.M. Sulaiman, M.A. Yarmo, F.A. Aziz, K.N. Ismail, N.S. Abdullah, Y. Abdullah, N.A. Rejabm, and M. Ahmadipour, Eds., vol. 888, Trans Tech Publications, Switzerland, 2017
5. H.R. Pasaribu, K.M. Reuver, D.J. Schipper, S. Ran, K.W. Wiratha, A.J.A. Winnubst, and D.H.A. Blank, Environmental Effects of Friction and Wear of Dry Sliding Zirconia and Alumina Ceramics Doped with Copper Oxide, *Int. J. Refract. Metals Hard Mater.*, 2005, **23**, p 386–390
6. A. Kovalcikova, P. Kurek, J. Balko, J. Dusza, P. Sajgalik, and M. Mihalikova, Effect of the Counterpart Material on Wear Characteristics of Silicon Carbide Ceramics, *Int. J. Refract. Metals Hard Mater.*, 2014, **44**, p 12–18
7. B. Kerkwijk, M. Garcia, W.E. Van Zyl, L. Winnubst, E.J. Mulder, D.J. Schipper, and H. Verweij, Friction Behaviour of Solid Oxide Lubricants as Second Phase in  $\alpha$ -Alumina and Stabilized  $ZrO_2$  Composites, *Wear*, 2004, **256**, p 182–189
8. B. Kerkwijk, A.J.A. Winnubst, H. Verweij, E.J. Mulder, H.S.C. Metselaar, and D.J. Schipper, Tribological Properties of Nanoscale Alumina-Zirconia Composites, *Wear*, 1999, **225–229**, p 1293–1302
9. A.K. Dey and K. Biswas, Dry Sliding Wear of Zirconia Toughened Alumina with Different Metal Oxide Additives, *Ceram. Int.*, 2009, **35**, p 997–1002
10. I. Akin, E. Yilmaz, F. Sahin, O. Yucel, and G. Goller, Effect of  $CeO_2$  Addition on Densification and Microstructure of  $Al_2O_3$ -YSZ Composites, *Ceram. Int.*, 2011, **37**, p 3273–3280
11. N.A. Rejab, A.Z.A. Azhar, M.M. Ratnam, and Z.A. Ahmad, The Relationship Between Microstructure and Fracture Toughness of Zirconia Toughened Alumina (ZTA) Added with MgO and  $CeO_2$ , *Int. J. Refract. Metals Hard Mater.*, 2013, **41**, p 522–530
12. R. Papitha, M. Buchi Suresh, and R. Johnson, High-Temperature Flexural Strength and Thermal Stability of Near Zero Expanding doped Aluminum Titanate Ceramics for Diesel Particulate Filters Applications, *Int. J. Appl. Ceram. Technol.*, 2014, **11**(4), p 773–782
13. A. Lyngfelt and T. Mattisson, *Materials for Chemical-Looping Combustion*, Wiley, Weinheim, 2011
14. L. Jedynak, J. Wojsa, J. Ojsa, J. Podwórny, and T. Wala, Refractories from the MgO- $Al_2O_3$ - $SnO_2$  System for Metallurgical Applications, *Ceram. Mater.*, 2011, **63**, p 34–39
15. J.-H. Liu, X.-J. Lv, J. Li, C. Zhang, Y.-Q. Lai, and Y.-X. Liu, Effect of MgO on Phase Compositions and Properties of  $Al_2O_3$ - $MgAl_2O_4$  Composite—A Prospective Man-Made Ledge Material, *Trans. Indian Ceram. Soc.*, 2016, **75**(2), p 108–111
16. Z. Harun, N.F. Ismail, and N.A. Badarulzaman, Effect of MgO Additive on Microstructure of  $Al_2O_3$ , *Adv. Mater. Res.*, 2012, **488–489**, p 335–339
17. F.Y. Zeng, Q.L. Wang, H. Liu, and X. Li, Synthesis and Characterization of Translucent MgO-Doped  $Al_2O_3$  Hollow Spheres in Millimeter Scale, *J. Alloys Compd.*, 2014, **608**, p 185–190
18. H.S.C. O'Neill and D.R. Scott, The Free Energy of Formation of  $Mg_2TiO_4$  (Synthetic Quandilite), an Inverse Spinel with Configurational Entropy, *Eur. J. Mineral.*, 2005, **17**, p 315–323
19. X. Xie, L. Guimin, D. Wei, Y. Wang, and Y. Jianguo, Effect of  $TiO_2$  on Melting and Crystallization Mechanism of Fused Magnesia, *Asian J. Chem.*, 2015, **27**(5), p 1823–1827
20. G. Kimmel, J. Zabicky, Stability, Instability, Metastability and Grain Size in Nanocrystalline Ceramic Oxide Systems, in *Solid State*

- Phenomena*, W. Łojkowski and J. R. Blizzard, Ed., vol. 140, Trans Tech Publications, Switzerland, 2008, pp. 29–36
21. K.T. Jacob, Gibbs Free Energies of Formation of  $ZnAl_2O_4$  and  $ZnCr_2O_4$ , *Thermochim. Acta*, 1976, **15**(1), p 79–87
  22. K.T. Jacob and C.B. Alcock, Thermodynamics of  $CuAlO_2$  and  $CuAl_2O_4$  and Phase Equilibria in the System  $Cu_2O$ - $CuO$ - $Al_2O_3$ , *J. Am. Ceram. Soc.*, 1975, **58**, p 192–195
  23. W. Hu, F. Donat, S.A. Scott, and J.S. Dennis, The Interaction Between  $CuO$  and  $Al_2O_3$  and the Reactivity of Copper Aluminates Below 1000 °C and Their Implication on the Use of the Cu-Al-O System for Oxygen Storage and Production, *RSC Adv.*, 2016, **6**, p 113016–113024
  24. C.-Y. Hu, K. Shih, and J.O. Leckie, Formation of Copper Aluminate Spinel and Cuprous Aluminate Delafossite to Thermally Stabilize Simulated Copper-Laden Sludge, *J. Hazard. Mater.*, 2010, **181**, p 399–404
  25. G.A. El-Shobaky, G.A. Fagal, and N.H. Amin, Thermal Solid-Solid Interaction Between  $CuO$  and Pure  $Al_2O_3$  Solids, *Thermochim. Acta*, 1989, **141**, p 205–216
  26. O. Tokariev, R.W. Steinbrech, L. Schnetter, and J. Malzbender, Micro- and Macro-mechanical Testing of Transparent  $MgAl_2O_4$  Spinel, *J. Mater. Sci.*, 2012, **47**, p 4821–4826
  27. R.V. Mangalaraja, B.K. Chandrasekhar, and P. Manohar, Effect of Ceria on the Physical, Mechanical and Thermal Properties of Yttria Stabilized Zirconia Toughened Alumina, *Mater. Sci. Eng. A*, 2003, **343**, p 71–75
  28. A. Goldstein, Y. Yeshurun, M. Vulfson, and H. Kravits, Fabrication of Transparent Polycrystalline  $ZnAl_2O_4$ —A New Optical Bulk Ceramic, *J. Am. Ceram. Soc.*, 2012, **95**, p 879–882
  29. N.R. Tedesco, E.M.J.A. Pallone, and R. Tomasi, Effects of the Pin on Disc Parameters on the Wear of Alumina, *Adv. Sci. Technol.*, 2010, **65**, p 39–44